Mar Geophys Res
DOI 10.1007/s11001-011-9142-0

ORIGINAL RESEARCH PAPER

Wave height characteristics in the Mediterranean Sea by means of numerical modeling, satellite data, statistical and geometrical techniques

George Galanis · Dan Hayes · George Zodiatis · Peter C. Chu · Yu-Heng Kuo · George Kallos

Received: 8 July 2011 / Accepted: 10 November 2011

Abstract In this paper the main wave height characteristics in the Mediterranean Sea are studied from both observational and numerical perspectives. The numerical wave model WAM is employed on a high spatial resolution mode and in two different versions, one of which incorporates information for sea surface currents. Altimeter data obtained from all available satellite missions over the area are also utilized. The data sets are analyzed both by conventional statistical measures as well as by advanced techniques provided by a relatively new branch of mathematics, information geometry, in the framework of which the data under study and the distributions that they form are treated as elements of non Euclidean spaces. In this framework, novel ideas for the estimation of the deviations between the observed and modeled values are proposed.

Keywords Numerical wave modeling · Significant wave height · Satellite altimeter data · Information geometry

G. Galanis (✉)
Section of Mathematics, Hellenic Naval Academy, Xatzikyriakion, 18539 Piraeus, Greece
e-mail: ggalanis@mg.uoa.gr

G. Galanis · G. Kallos
Department of Physics, Atmospheric Modeling and Weather Forecasting Group, University of Athens, University Campus, Bldg. PHYS-V, 15784 Athens, Greece

D. Hayes · G. Zodiatis
Oceanography Centre, University of Cyprus, 1678 Nicosia, Cyprus

P. C. Chu · Y.-H. Kuo
Department of Oceanography, Naval Postgraduate School, Graduate School of Engineering and Applied Science, Monterey, CA 93943, USA

Introduction

Recent developments and advances in the environmental sciences have increased the interest and the necessity for systems able to accurately monitor and predict meteorological/oceanographic parameters. The main tools that the research community have available today in order to respond adequately to the above issues are two: Observation networks, that record the evolution of the parameters of interest, and mathematical/physical models which simulate their evolution in time and space. The level of difficulty in both approaches increases when focusing on sea wave characteristics: We still lack a dense observational network, analogous to the existing one over land areas, able to provide systematic observations at a sufficient resolution. This fact underlines the importance of satellite data. On the other hand, wave modeling seems to be incomplete without being coupled with atmospheric and currents flow corresponding systems.

In the present work a study of the sea wave characteristics in the area of Mediterranean Sea has been attempted. In particular, the spatial and temporal distribution of significant wave height was studied from different points of view: numerical modeling and satellite records.

The former approach is based on the use of a state of the art numerical wave prediction system: the WAM model (WAMDIG 1988; Komen et al. 1994; Janssen 2000, 2004; Bidlot et al. 2007; Galanis et al. 2006, 2009; Emmanouil et al. 2007). This is one of the most well tested wave models being used today by several operational and research centres. The model's domain was covering the whole Mediterranean region at a horizontal resolution of 0.05° for one year (2009). In addition, a second version of the model implementing in the simulation procedure information concerning the sea surface currents has been

Published online: 26 November 2011

used. The potential benefits for the wave model are investigated. Both model versions are evaluated/compared against corresponding satellite measurements obtained by all available missions in the area (Radar Altimetry project, Rosmorduc et al. 2009).

The intercomparison between these independent sources of data provides information both for the Mediterranean Sea wave characteristics and the forecasting abilities of the wave model. It should be noted however, that no climatic generalizations or interannual comparisons could be made since only one year of data have been analyzed.

Two different statistical approaches are employed: one adopting conventional methods in which the most representative descriptive statistical indexes describing the wave characteristics are analyzed, and a second focusing on the probability density functions that fit to the data under study. The second approach reveals non trivial deviations between the modeled and recorded data that should be essentially taken into account in assimilation or other optimization procedures (Lionello et al. 1992, 1995; Breivik and Reistad 1994; Janssen 2000; Kalnay 2002; Abdalla et al. 2005a, b; Galanis et al. 2006, 2009). In this framework, advances from a new branch of mathematics, information geometry (Amari 1985; Amari and Nagaoka 2000; Arwini and Dodson 2007, 2008), are employed in order to optimally estimate the distances between different data sets.

Special attention is given to the Levantine region (the sea area with longitude 30–37° and latitude 31–37° defined by the red rectangle in Fig. 1), in which the homogeneous wave characteristics allow to test/discuss the proposed techniques avoiding lumping non compatible information.

The techniques and ideas proposed in this work could be exploited for designing new methods for the optimization of the initial conditions and the final outputs of numerical wave and atmospheric prediction systems since they could support more sophisticated ways of realizing the corresponding cost functions taking into account the geometric properties (scale and shape parameters for example) of the data in study and avoiding simplifications that the classical approaches (least square methods) impose.

The presented work is organized as follows: In "Models and methodology" the models, the data sets and the methodology used is described. "Wave modeling" is devoted to the wave model employed, "Satellite data" refers to the satellite records utilized, while "Statistical approaches: methodology" focuses on the statistical approaches adopted. In "Results"and "Information geometric techniques for the distance estimation between observations and forecasts" the results obtained in this study are presented and discussed focusing mainly on the new techniques proposed for the estimation of the distance between observations and forecasts based on information geometric techniques. Finally, concluding thoughts are summarized in "Conclusions".

Models and methodology

Wave modeling

The third generation wave model model WAM Cycle 4—ECMWF version (Janssen 2000, 2004; Bidlot et al. 2007) is used for simulating the evolution of the significant wave height in Mediterranean Sea. WAM solves the wave transport equation explicitly without any assumptions on the shape of the wave spectrum (WAMDIG 1988; Komen et al. 1994). It computes the 2-d wave variance spectrum through integration of the transport equation:

$$\frac{\mathrm{d}F}{\mathrm{d}t}+\frac{\partial}{\partial\varphi}(\dot{\varphi}F)+\frac{\partial}{\partial\lambda}(\dot{\lambda}F)+\frac{\partial}{\partial\theta}(\dot{\theta}F)=S,$$

where $F(\mathrm{f},\theta,\varphi,\lambda)$ denotes the spectral density, f frequencies, θ directions, φ latitudes and λ longitudes. The source function S is represented as a superposition of the wind input S_{in}, white capping dissipation S_{dis}, and nonlinear transfer S_{nl}:

$$S = S_{in} + S_{dis} + S_{nl}$$

The wind input term is given by

$$S_{in} = \gamma F,$$

with γ the growth rate of the waves. The dissipation source term is based on (Hasselmann 1974) white capping theory according to (Komen et al. 1984). The nonlinear source term is a parameterization of the exact nonlinear interactions as proposed by (Hasselmann et al. 1985). The basic form of the exact nonlinear expression has been retained. However the 5-d continuum of all resonant quadruplets is reduced to a 2-d continuum by considering only a pair of discrete interaction configurations. More details on the theoretical background on which the WAM model is based can be found in (WAMDIG 1988).

It is worth also mentioning on the new advection scheme used in the latest version (CY33R1) of the wave model that ECMWF has kindly provided to our group (Bidlot et al. 2007). The corner transport upstream has been adopted replacing the original scheme for oblique propagation. There is also a change in the non-linear source term expression for shallow water. Based on a recent work of Janssen and Onorato 2007), concerning the effects of four wave interactions and the generation of a wave-induced current, the new scheme affects both the time evolution of the wave spectrum and the determination of the kurtosis of the wave field.

The model ran for a period of 12 months (year 2009) covering the whole Mediterranean Sea (Latitude 30°N–46°N, Longitude 6°W–36°E, Fig. 1) at a high—for a basin-scale model—spatial resolution (0.05°, that is around 4.3 km in longitude differences and 5.5 km in latitude)

Fig. 1 The area of interest. The *red rectangle* indicates the restricted area of study (Levantine Sea). *Image* courtesy of Google Earth

providing outputs at 6-h intervals in order to capture the details of the evolution of sea waves even in areas with a complicated coast line. The wave spectrum was discretized to 25 frequencies (range 0.0417–0.54764 Hz logarithmically spaced) and 24 directions (equally spaced) while the propagation time step was 120 s. Since the domain of the model covers the whole Mediterranean Sea, WAM was operated in a deep water mode with not bottom refraction, driven by 3-h wind input (10 m wind speed and direction) obtained from the SKIRON regional atmospheric system (Kallos 1997; Papadopoulos et al. 2001) that runs operationally once a day (with 12 UTC initial conditions) at the University of Athens providing 5-day forecasts.[1] The horizontal resolution used for SKIRON system coincides with that of the wave model ($0.05 \times 0.05°$) while 45 vertical levels stretching from surface to 20 km are employed. The atmospheric system uses NCEP/GFS $0.5 \times 0.5°$ resolution fields for initial and boundary conditions. The necessary sea surface boundary conditions are interpolated from the $0.5 \times 0.5°$ SST (Sea Surface Temperature) field analysis retrieved from NCEP on daily basis. Vegetation and topography data are applied at a resolution of 30 s and soil texture data at 120 s.

In addition, a second version of the wave model (WAMC for convenience in the following) was employed in which apart from the wind forcing, surface wave currents were also used. In particular, their propagation characteristics both spatially and spectrally (current refraction, frequency bunching) where taken into account. The two horizontal components of the surface sea currents at a resolution of 1/16°, approximately 6 km, were provided by the Mediterranean Operational Oceanography Network—MOON basin system, known as Mediterranean Forecasting System-MFS (Pinardi et al. 2003). This forecasting system produces daily means of sea temperature and salinity forecasts, with 10-days forecasting horizons, on a daily basis. The system consists of a numerical model (Tonani et al. 2008) and a data assimilation scheme (3DVAR) (Dobricic and Pinardi 2008) capable of assimilating satellite and in situ data. MFS is forced by atmospheric input produced by the European Center for Medium range Weather Forecasts (ECMWF) analyses and forecasts (ECMWF 2005) at $0.5 \times 0.5°$ and 6 h resolution. The MFS forecasts are validated/compared with observations, providing an assessment of the forecasting products.

Satellite data

Gridded observational records from the ESA-CNES joint project Radar Altimetry Tutorial were used as observation data. These are near-real time observations for significant wave height obtained by merging all available relevant

[1] http://www.mg.uoa.gr/

satellite records from a variety of data centers: ERS-1 and ERS-2 (ESA), Topex/Poseidon (NASA/CNES), Geosat Follow-On (US Navy), Jason-1 (CNES/NASA), Envisat (ESA). In particular, the last 2 days of available data for each satellite are employed and a merged map is generated on daily basis if a minimum of two missions is available. The final outputs are obtained by means of interpolation and cover the area of study for the year 2009 at a resolution of 0.25°. Cross-calibration and quality control of the data are performed using Jason-1 as the reference mission (Rosmorduc et al. 2009). Concerning the accuracy of the satellite data in use, it is well known that bias uncertainty is always a non negligible factor in altimeter error budgets. A variety of factors contribute to this issue: Measurement noise, which depends on the antenna baseline, the error related to ionospheric, tropospheric and sea-state bias effects, the error induced by satellite roll and pitch, which has a direct impact on measurement geometry (Yaplee et al. 1971; Enjolras et al. 2006). However, the fact that the data used in the present study have been resulted within the framework of a major European project coordinated by the European Space Agency and were calibrated against independent measurements provides an important guarantee for their credibility. In particular, the estimated order of magnitude for the bias is from 0 to 50 cm, depending on wave heights (Rosmorduc et al. 2009).

The choice of the specific year 2009 has been imposed mainly by data availability reasons. Although this is a statistically sufficient period for obtaining safe results and giving a description of the proposed new techniques, it should be noted that no climatic generalization is asserted.

It worth also noticing that a non-trivial difference in the temporal and spatial resolution between the modeled and recorded wave data is present, which, despite the interpolation used for spreading the available information in the framework of Radar Altimetry Tutorial project, may result to sampling error in the analysis. For this reason, our study and results focus on averaged statistical parameters over quarterly periods, during which a sufficient amount of satellite records are available and the previously mentioned errors are eased, avoiding to provide estimations for short time periods or restricted local areas. Despite this, a, possibly systematic, bias could be expected and this underlines the necessity of developing new advanced techniques for the estimation and the subsequent elimination of such discrepancies. This is exactly the framework in which the proposed methodologies aim to provide some new material and ideas.

Another point that is mentionable is the recent evidence that wave data from Jason-1 are quite noisy and may not be the best reference there is (see for instance Abdalla et al. 2005a, b; Durrant et al. 2009). An alternative could be provided by the GlobWave project (http://www.globwave.org/) in the framework of which data from different satellite missions are also available.

Statistical approaches: methodology

Two complementary methodologies are used for the statistical analysis of both observations and wave simulations. Firstly, conventional statistical measures provide the basic information for the significant wave height distribution in time and space. More precisely, the following indices were used:

- *Mean value* $\mu = \frac{1}{N} \times \sum_{i=1}^{N} swh(i)$, were *swh* denotes the recorded (observed) or simulated significant wave height value and *N* the size of the sample.
- *Standard Deviation* $\sigma = \sqrt{\frac{1}{N} \times \sum_{i=1}^{N} (swh(i) - \mu)^2}$
- *Coefficient of variation* $c_v = \frac{\sigma}{\mu}$, a normalized measure of the dispersion.
- *Skewness* $g_1 = \frac{\frac{1}{N} \times \sum_{i=1}^{N} (swh(i) - \mu)^3}{\sigma^3}$ a measure of the asymmetry of the probability distribution.
- *Kurtosis* $g_2 = \frac{\frac{1}{N} \times \sum_{i=1}^{N} (swh(i) - \mu)^4}{\sigma^4} - 3$ that provides information about the "peakedness" of the probability distribution.
- The basic percentiles: P_5, P_{10}, $P_{25} = Q_1$, $P_{50} =$ Median, $P_{75} = Q_3$, P_{90} and P_{95}, that give a detailed view of the distribution of the data in study.

It should be noted that the wave data have been descritized in daily averages to the statistical metrics used in order to analyze in a homogeneous way the modeled and recorded values.

The second statistical approach is based on information geometry, a relatively new research area with several potential applications that surpass the classical borders of mathematics. In order to make this work as self-contained as possible, a short presentation of the main notions and terminology of information geometric techniques follows. More details and results can be found in Amari 1985; Amari and Nagaoka 2000; Arwini and Dodson 2007, 2008.

The primary scope is to exploit methods of non-Euclidean geometry in probability theory and stochastic processes. The information geometry provides a manifold framework for a family of probability distributions. Within this, geometrical entities such as Riemannian metrics and distances are introduced. For example, the family of normal distributions of 1-d variables can be treated as a two dimensional manifold where the mean and variance playing the role of coordinates.

The main objects of information geometry are the statistical manifolds. Namely, an *n*-dimensional statistical manifold is a family of probability distributions

$$S = \{p_\xi = p(x;\xi) | \xi = [\xi_1, \xi_2, \ldots, \xi_n] \in \Xi\} \quad (1)$$

where each element may be parametrized using the n real valued variables $[\xi_1, \xi_2, \ldots, \xi_n]$ in an open subset Ξ of $\mathbb{R}^n$ and the mapping $\xi \to p_\xi$ is injective and smooth.

The geometrical framework of a statistical manifold is given by the *Fisher information matrix* which at a point ξ is a $n \times n$ matrix

$$G(\xi) = [g_{ij}(\xi)], \quad (2)$$

with

$$\begin{aligned} g_{ij}(\xi) &= E_\xi[\partial_i \ell(x;\xi)\partial_j \ell(x;\xi)] \\ &= \int \partial_i \ell(x;\xi)\partial_j \ell(x;\xi) p(x;\xi)\mathrm{d}x, \\ i,j &= 1,2,\ldots,n. \end{aligned} \quad (3)$$

Here ∂_i stands for the partial derivative with respect to the i-th factor, ℓ is the log-likelihood function:

$$\ell(x;\xi) = \ell_\xi(x) = \log[p(x;\xi)] \quad (4)$$

and

$$E_\xi[f] = \int f(x) p(x;\xi)\mathrm{d}x \quad (5)$$

denotes the expectation with respect to the distribution p.

The matrix $G(\xi)$ is always symmetric and positive semi-definite. If, in addition, it is positive definite, then a Riemannian metric (see Spivak 1965, 1979) can be defined on the statistical manifold corresponding to the induced inner product:

$$g_{ij} = \langle \partial_i | \partial_j \rangle. \quad (6)$$

This Riemannian metric is called the *Fisher metric* or the *information metric* and is invariant of the choice of the coordinate system. The corresponding geometric properties of this framework are characterized by the so-called Christoffel symbols (Γ^i_{jk}) defined by the relations:

$$\Gamma_{jk,h} = \sum_{i=1}^{2} g_{hi}\Gamma^i_{jk}(\mathrm{h} = 1,2), \quad (7)$$

$$\begin{aligned} \Gamma_{jk,h}(\xi) &= E_\xi\left[\left(\partial_j\partial_k\ell_\xi + \frac{1}{2}\partial_j\ell_\xi\partial_k\ell_\xi\right)(\partial_h\ell_\xi)\right], \\ i,j &= 1,2,\ldots,n. \end{aligned} \quad (8)$$

The minimum distance between two elements f_1 and f_2 of a statistical manifold S is defined by the corresponding *geodesic* ω which is the minimum length curve that connects them. Such a curve

$$\omega = (\omega_i) : \mathbb{R} \to S \quad (9)$$

satisfies the following system of 2nd order differential equations:

$$\omega_i''(t) + \sum_{j,k=1}^{n} \Gamma^i_{jk}(t)\omega_j'(t)\omega_k'(t) = 0, \quad i = 1,2,\ldots,n. \quad (10)$$

under the conditions $\omega(0) = f_1, \omega(1) = f_2$.

It is worth noticing at this point, that the above presented framework of information geometric techniques has been exploited so far in a variety of applications in biology and mathematical physics (see Amari and Nagaoka 2000; Arwini and Dodson 2007, 2008). However, to the authors' knowledge, similar applications in meteorology and oceanography are still missing, although optimization and assimilation procedures are widely utilized.

Results

Descriptive statistics

The significant wave height characteristics over the whole Mediterranean Sea are studied here based on the descriptive statistical measures listed in the previous section. In order to differentiate between non homogeneous time periods, the data in study (both model results and satellite observations) have been divided in four intervals corresponding to the seasons: Period A covers the winter months (December–February), B the spring (March–May), C the summer (June–August) and D the autumn (September–November).

In Figs. 2, 3, 4 and 5, the average values of the mean, the standard deviation, the skewness and the kurtosis over every grid point of the domain are presented for the two versions of the wave model (with and without the currents as external information) and the satellite records.

The use of the sea surface currents (WAMC) does not change significantly the results of the model simulation since the corresponding statistics are, in general, similar. However, it does increase the mean significant wave height (swh) values as well as the corresponding variability, as expressed by the standard deviation, at specific areas like the Southern France coastline especially during winter months. The elevated variability, in particular, indicates that the increased swh may not be the case for the whole area or time of study.

A second interesting outcome concerns the elevated kurtosis values of the model results. This deviation is particularly apparent during the summer period and reveals increased influence of extreme values on the variability of the forecasts. In general, for the western Mediterranean, the study seems to indicate non-uniform distributions of swh (both from skewness and a kurtosis point of view). The Levantine region is affected mainly during the autumn

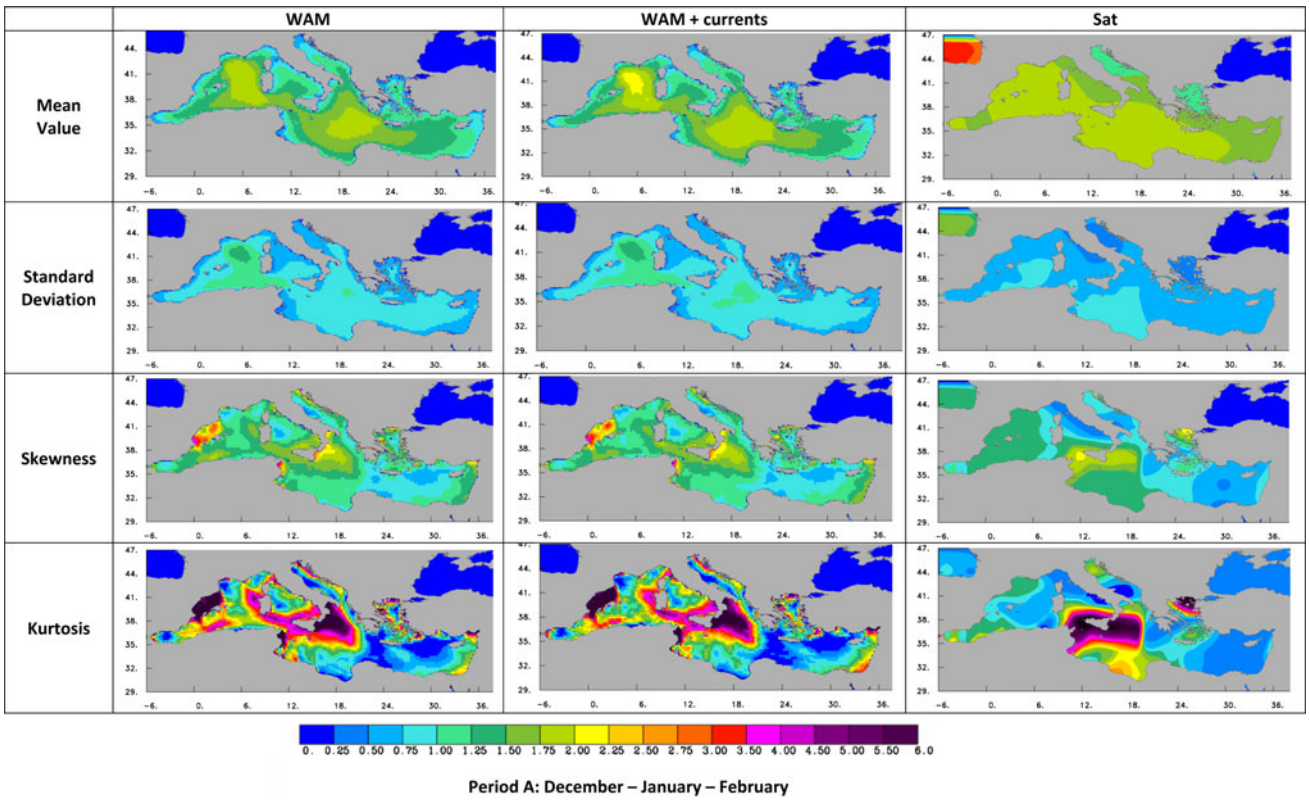

Fig. 2 Basic statistical measures for the two model version: with (WAMC) and without (WAM) current information, as well as for the corresponding satellite records for the months December–February

period when both the models and the observations agree on the increased values for the two asymmetry measures.

The previous information is important especially for applications related with wave energy activities since swh is a crucial component in energy potential estimation. It is worth noticing here that the statistical analysis for the modeled results is based on a wider sample due to the finer resolution (both spatial and temporal) compared to the available satellite records. It is underlined, in this way, the added value of numerical modeling especially in regions with limited available observations.

Some more specific conclusions can be made for Levantine due to the relatively homogeneous wave climate. In Figs. 6, 7, 8 and 9 the statistical measures employed are graphically presented in monthly intervals while the relevant percentiles are given in Tables 1, 2 and 3. The model generally underestimates swh, especially in winter. This bias is improved, at least partly, by the use of sea currents. On the other hand, model results (both with and without currents) are more variable and asymmetric, especially during the winter months, compared to the satellite measurements. Beside this, some questions rise for the extrapolation of the satellite data: the mean difference between the model outputs and the observations seems to be too large, which combined with a lack of variability and extremes in the altimeter data it points to a data set that has been heavily smoothed and extrapolated. It is worth noticing at this point that the figures under discussion (6–9) are referring on the available values over the whole Levantine area (longitude 30–37 and latitude 31–37° at a horizontal resolution of 0.05°). As a result a statistical sufficient sample size is ensured.

Probability density function fitting

In this section, the swh satellite records and the corresponding WAM simulations are studied by distribution fitting. Wave data have been fitted at a significance level of 0.05 or higher (D'Agostino and Stephens 1986) to the two-parameter Weibull probability density function:

$$f(x) = \frac{\alpha}{\beta}\left(\frac{x}{\beta}\right)^{\alpha-1} \mathrm{e}^{-\left(\frac{x}{\beta}\right)^{\alpha}}, \quad \alpha, \beta > 0, \tag{11}$$

where α is the shape and β the scale parameter. This distribution has been proved to describe well sea waves in a number of previous works (Holthuijsen 2007; Muraleedharan et al. 2007).

In Figs. 10, 11, 12 and 13 the values of the shape and scale parameter, divided again in four seasons, over every grid point of the domain are plotted for the two WAM

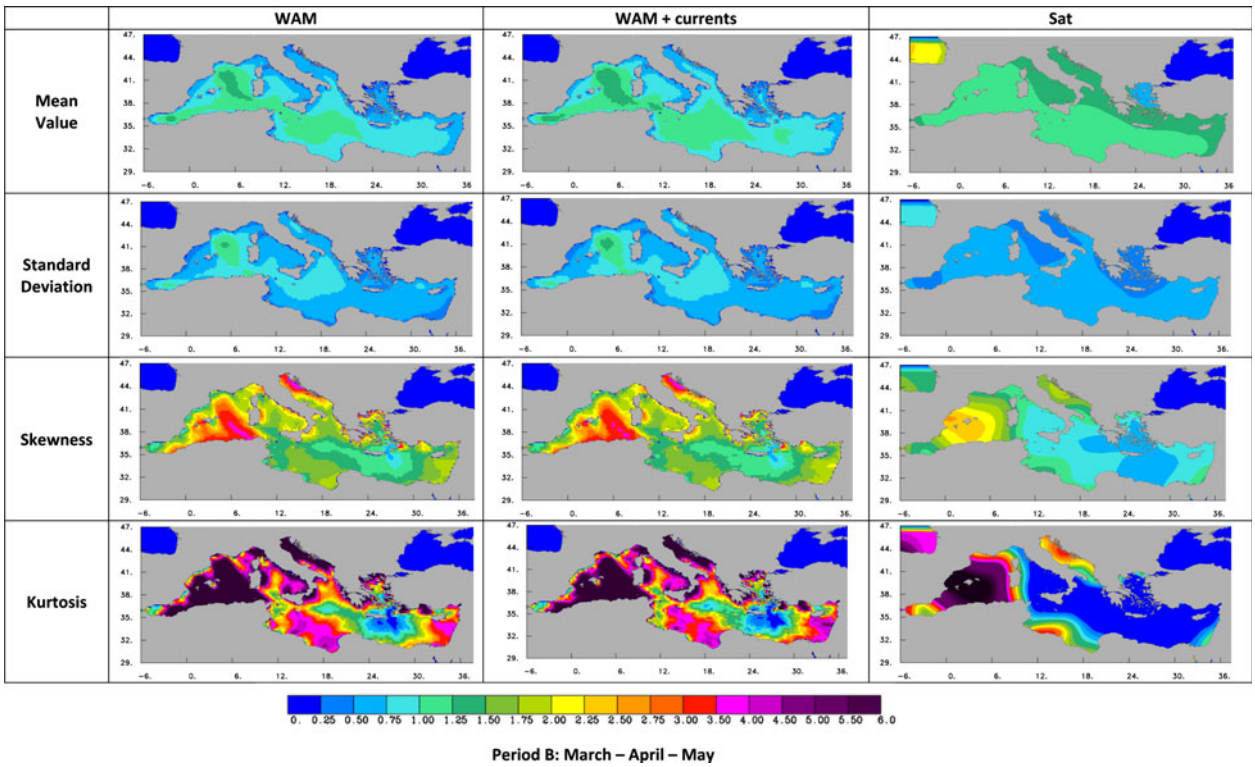

Fig. 3 Basic statistical measures for the two model versions: with (WAMC) and without (WAM) current information, as well as for the corresponding satellite records for the months March–May

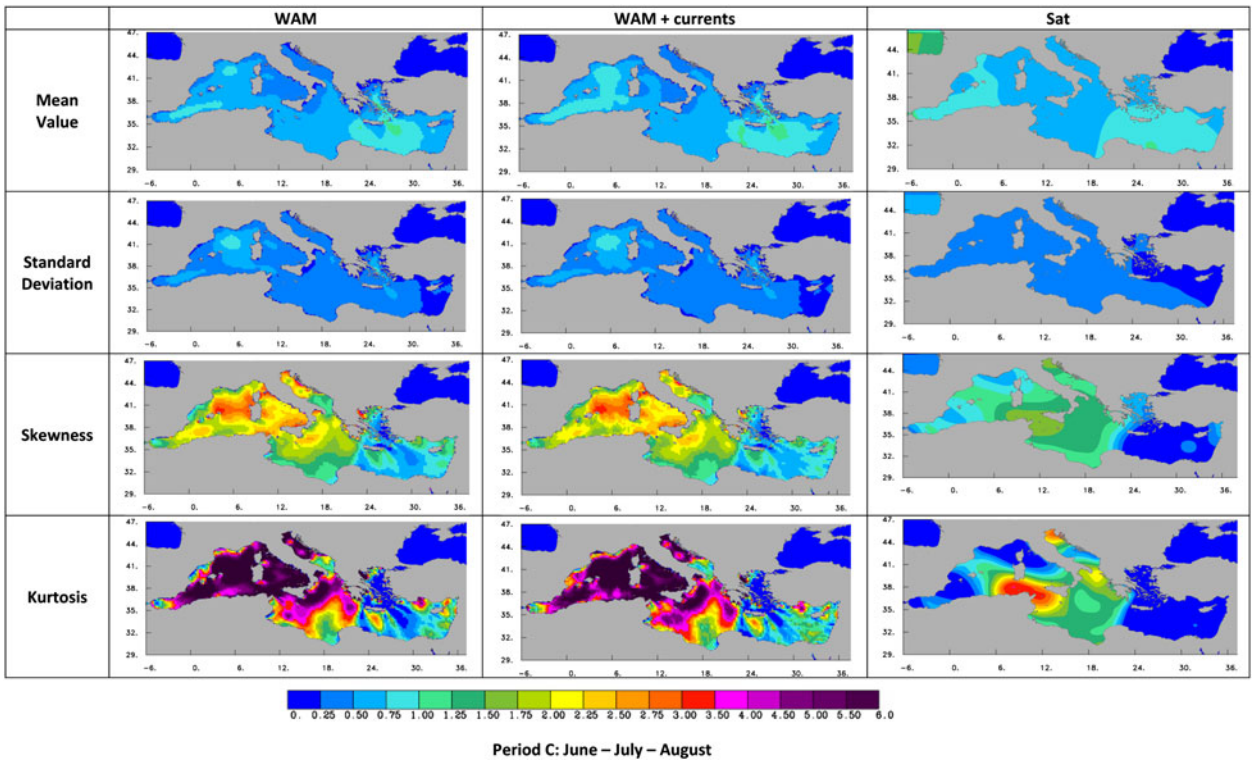

Fig. 4 Basic statistical measures for the two model versions: with (WAMC) and without (WAM) current information, as well as for the corresponding satellite records for the months June–August

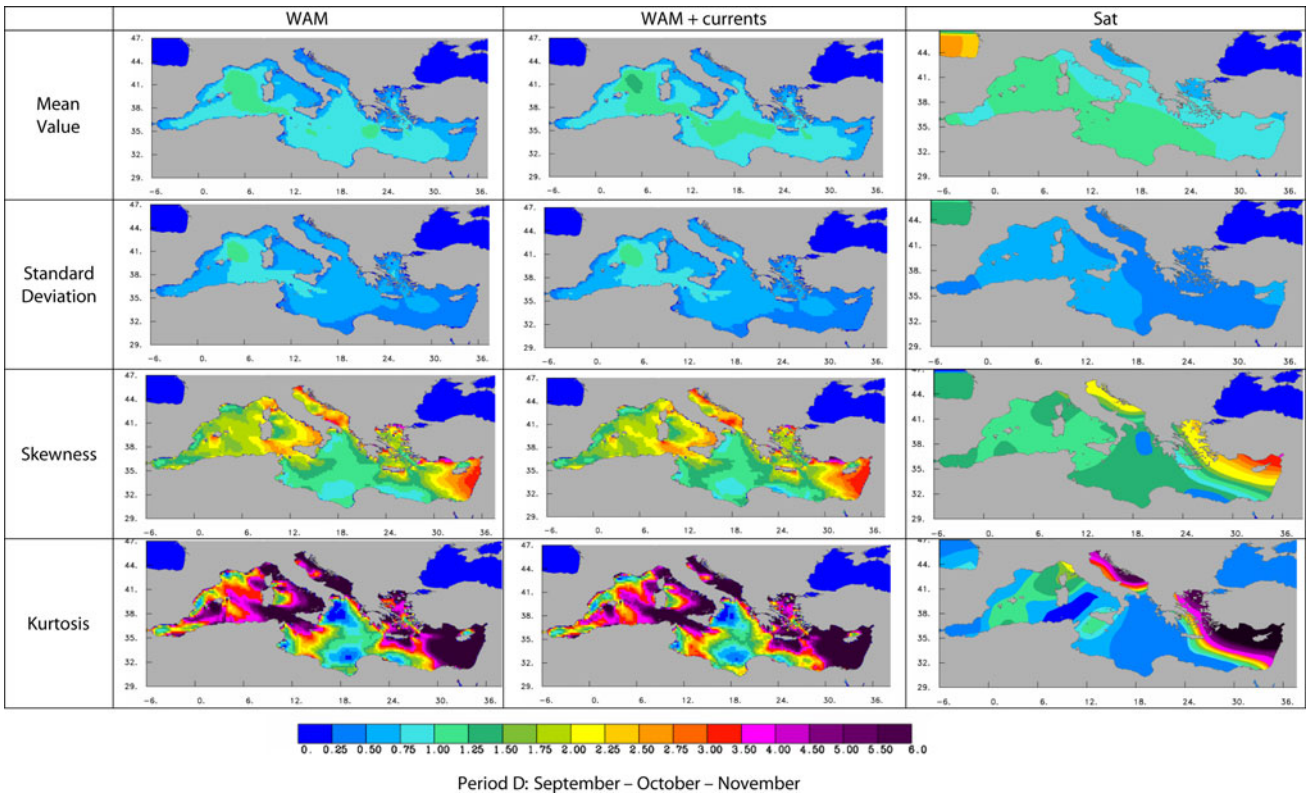

Fig. 5 Basic statistical measures for the two model versions: with (WAMC) and without (WAM) current information, as well as for the corresponding satellite records for the months September–November

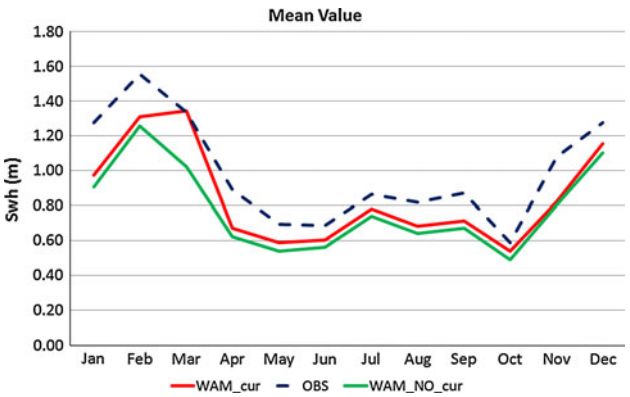

Fig. 6 The time evolution of the mean swh in the Levantine area

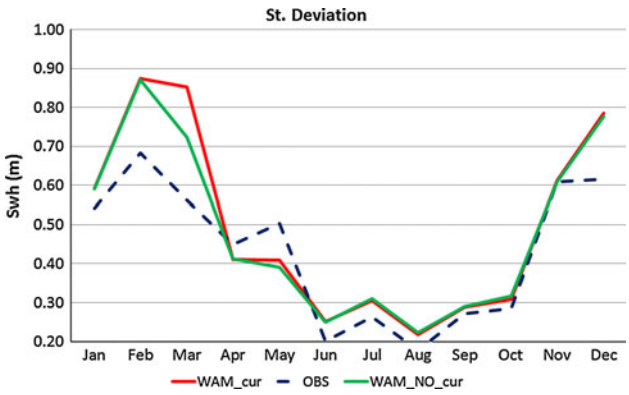

Fig. 7 The time evolution of the standard deviation of the swh in the Levantine area

versions: including current information (WAMC) and not (WAM) as well as for the corresponding satellite records. The main outcome here is the increased shape parameter values for the satellite records over the whole time period and almost at every area of the Mediterranean Sea. This fact underlines the qualitatively different characteristics between the modeled and measured data that should be taken into account in any optimization procedure (assimilation, local adaptation, etc.). The same holds also for the spatial variability of the results. Elevated shape and scale parameters are revealed during winter in regions with relatively large potential fetch (Ionian sea, southern France to northern Africa). A second important observation is the increased values of the shape parameter in the Levantine area during the summer period as simulated by both versions of the WAM model and recorded by the satellites.

More detailed results (monthly averages) for the Levantine area are presented in Figs. 14 and 15 where the evolution in time for the shape and scale parameter of the

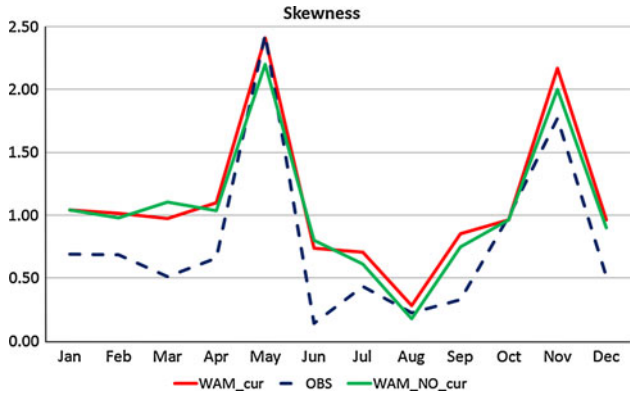

Fig. 8 The time evolution of the skewness of the swh in the Levantine area

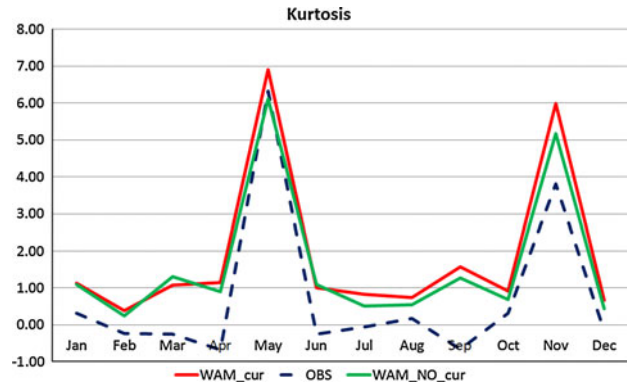

Fig. 9 The time evolution of the kurtosis of the swh in the Levantine area

Weibull pdf is given. The underestimation of the shape parameters by WAM is reconfirmed and is particularly obvious during the summer months. On the other hand, the systematic underestimation of the scale parameter is in accordance with the decreased mean modeled values in this area (Fig. 6). Again, the use of sea current information in the wave model does not seem to affect crucially the above findings. The statistical significance of these conclusions is supported by the 95% confidence intervals presented in Tables 4, 5 and 6. Indeed, very limited intervals (with lengths <0.1) is the case for the modeled data (Tables 4, 5) while a slightly increased variation is allowed for the satellite records which, however, is not enough to set under question the discrepancies from the WAM results.

Information geometric techniques for the distance estimation between observations and forecasts

The results obtained in the previous sections reveal non negligible deviations between the modeled and recorded swhs as well as remarkable spatial distribution. This is not something new. Many authors over the years have pointed out possible causes leading the numerical prediction systems to produce errors systematic or not (Janssen et al. 1987; Kalnay 2002; Chu et al. 2004; Greenslade and Young 2005; Galanis et al. 2006; Chu and Cheng 2007, 2008; Emmanouil et al. 2007; Galanis et al. 2009). The local area's peculiarities, the heavy dependence on the initial conditions (mainly for the atmospheric models, see for example Bertotti et al. 2011) and the inability to simulate successfully sub-grid scale phenomena can be listed among them. On the other hand, one should not forget that altimeter data have also errors that tend to be of the same level on a global scale to that of global wave models (Janssen et al. 2007; Abdalla et al. 2010). These facts set under question the way that conventional statistical procedures are employed in order to estimate and minimize the distances between the two types of data sets. Indeed, in the majority of assimilation and other optimization techniques (Kalman 1960; Kalman and Bucy 1961; Lionello et al. 1992, 1995; Breivik and Reistad 1994; Rao et al. 1997; Galanis and Anadranistakis 2002; Kalnay 2002; Makarynskyy 2004, 2005; Abdalla et al. 2005a, b), the obtained "cost-functions" treat the data in study as elements of Euclidean spaces by employing different versions of the least square method. However, novel advances in a new branch of mathematics, the information geometry,

Table 1 Monthly swh values for the percentiles of the WAM (no currents) version for the area of Levantine

Percentile	Jan	Feb	Mar	Apr	May	Jun	Jul	Aug	Sep	Oct	Nov	Dec	Overall
Min	0.07	0.07	0.07	0.07	0.07	0.07	0.07	0.07	0.07	0.07	0.07	0.07	0.07
5%	0.18	0.24	0.18	0.09	0.12	0.2	0.31	0.27	0.23	0.11	0.16	0.16	0.19
10%	0.27	0.35	0.26	0.15	0.18	0.26	0.4	0.37	0.34	0.14	0.24	0.23	0.27
25% (Q1)	0.45	0.59	0.44	0.32	0.32	0.38	0.53	0.51	0.48	0.24	0.41	0.48	0.43
50% (Median)	0.79	1.01	0.86	0.54	0.45	0.53	0.7	0.64	0.64	0.41	0.64	0.94	0.68
75% (Q3)	1.24	1.74	1.44	0.83	0.62	0.7	0.93	0.77	0.82	0.69	1.01	1.56	1.03
90%	1.72	2.6	2.05	1.21	0.95	0.9	1.2	0.92	1.05	0.93	1.48	2.25	1.44
95%	2.05	3.07	2.44	1.47	1.4	1	1.3	1.02	1.21	1.1	2.07	2.65	1.73
Max	4.15	4.68	5.74	2.61	2.8	2.1	2.2	1.79	2.18	2.1	4.15	5.4	3.33

Table 2 Monthly swh values for the percentiles of the WAMC version for the area of Levantine

Percentile	Jan	Feb	Mar	Apr	May	Jun	Jul	Aug	Sep	Oct	Nov	Dec	Overall
Min	0.04	0.04	0.04	0.03	0.04	0.04	0.04	0.03	0.04	0.04	0.04	0.04	0.04
5%	0.25	0.31	0.27	0.26	0.18	0.25	0.36	0.26	0.3	0.16	0.23	0.21	0.25
10%	0.34	0.41	0.34	0.39	0.25	0.31	0.44	0.39	0.4	0.2	0.31	0.29	0.34
25% (Q1)	0.52	0.64	0.52	0.69	0.37	0.42	0.57	0.69	0.52	0.3	0.43	0.53	0.52
50% (Median)	0.86	1.07	0.92	1.18	0.49	0.58	0.74	1.18	0.67	0.47	0.64	0.98	0.82
75% (Q3)	1.3	1.77	1.49	1.85	0.65	0.75	0.95	1.85	0.86	0.73	1.03	1.62	1.24
90%	1.8	2.66	2.13	2.49	0.99	0.93	1.2	2.49	1.1	0.97	1.48	2.29	1.71
95%	2.12	3.15	2.55	2.93	1.55	1.05	1.34	2.93	1.25	1.12	2.04	2.72	2.06
Max	4.08	4.68	5.8	5.98	3.34	2.19	2.36	5.98	2.34	2.19	4.55	5.58	4.09

Table 3 Monthly swh values for the percentiles of the satellite data for the area of Levantine

Percentile	Jan	Feb	Mar	Apr	May	Jun	Jul	Aug	Sep	Oct	Nov	Dec	Overall
Min	0.30	0.38	0.35	0.19	0.11	0.19	0.27	0.35	0.26	0.13	0.29	0.28	0.26
5%	0.52	0.69	0.54	0.38	0.27	0.37	0.45	0.53	0.49	0.25	0.44	0.38	0.44
10%	0.63	0.77	0.62	0.41	0.34	0.42	0.54	0.59	0.54	0.29	0.50	0.47	0.51
25% (Q1)	0.86	0.98	0.86	0.52	0.41	0.53	0.68	0.71	0.64	0.36	0.64	0.83	0.67
50% (Median)	1.20	1.43	1.33	0.71	0.52	0.69	0.83	0.82	0.85	0.53	0.96	1.22	0.93
75% (Q3)	1.60	2.09	1.68	1.30	0.73	0.82	1.06	0.92	1.05	0.73	1.28	1.67	1.24
90%	2.05	2.48	2.12	1.53	1.27	0.94	1.22	1.04	1.27	1.04	1.69	2.08	1.56
95%	2.17	2.84	2.38	1.71	1.88	1.01	1.31	1.13	1.36	1.22	2.48	2.54	1.84
Max	3.29	3.53	3.07	2.28	2.94	1.41	1.73	1.37	1.65	1.40	4.02	3.12	2.48

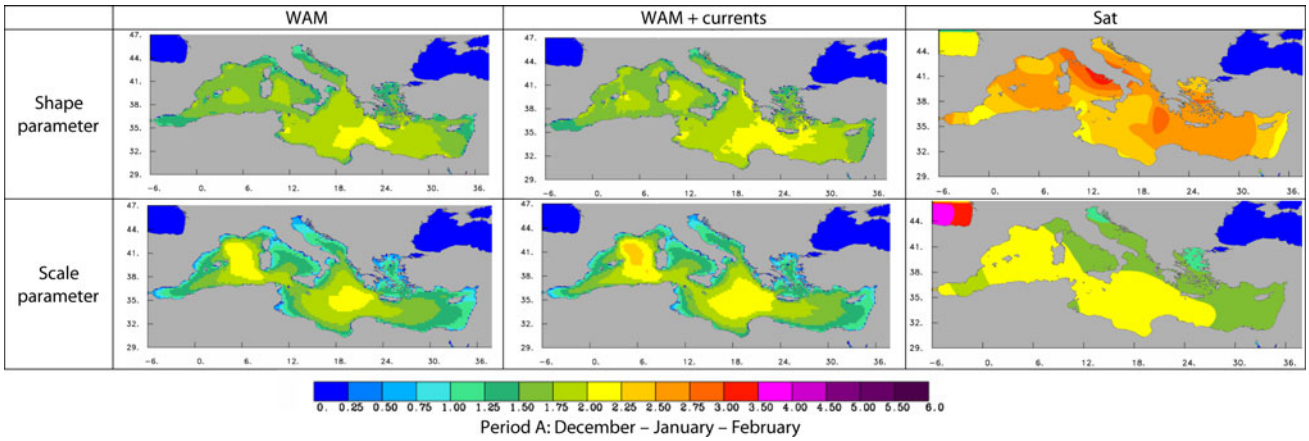

Fig. 10 The *shape* and *scale* parameter for the two model versions: with (WAMC) and without (WAM) current information, as well as for the corresponding satellite records for the months December–February

prove that such an approach contains serious limiting and simplifications. This is because the distributions of data sets normally are classified in more complicated structures than Euclidean spaces, in which the underlying geometry differ from the classical one (see Amari 1985; Amari and Nagaoka 2000; Arwini and Dodson 2007, 2008). In particular, probability density functions of the same type form differentiable Riemannian manifolds (Spivak 1965, 1979) which can be explicitly defined following standard protocols. Such a description provides a different way for the estimation of distances, since within the Riemannian geometry framework the distance between two elements is given as the length of the geodesic, i.e. the minimum length curve, which is not always a straight line. These new tools can provide more accurate criteria and procedures for the optimization of the model final results.

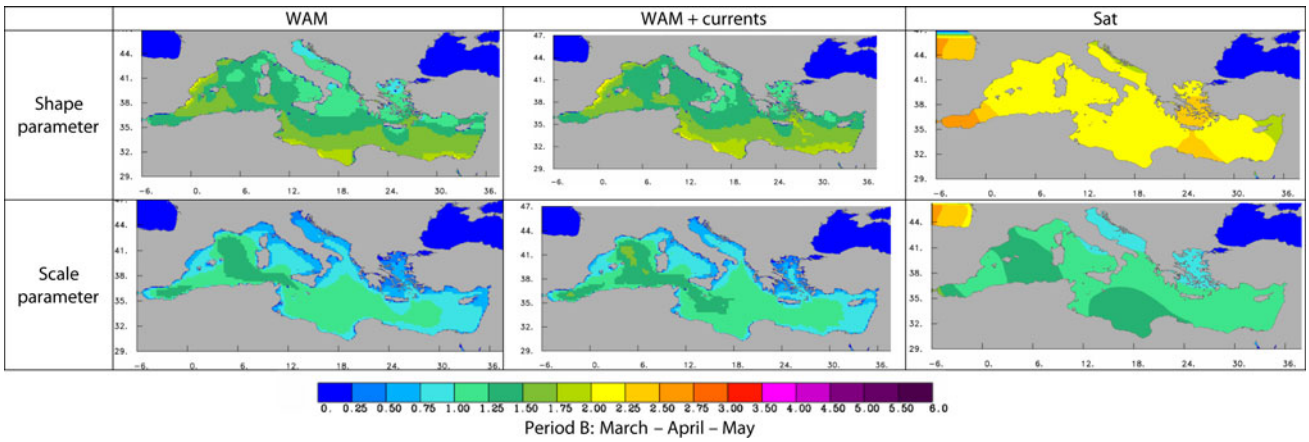

Fig. 11 The *shape* and *scale* parameter for the two model versions: with (WAMC) and without (WAM) current information, as well as for the corresponding satellite records for the months March–May

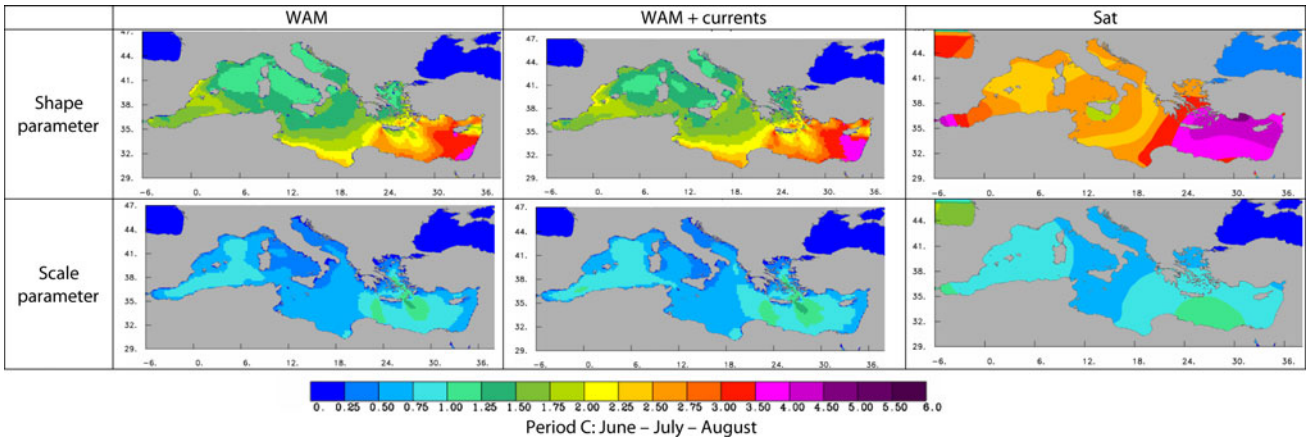

Fig. 12 The *shape* and *scale* parameter for the two model versions: with (WAMC) and without (WAM) current information, as well as for the corresponding satellite records for the months June–August

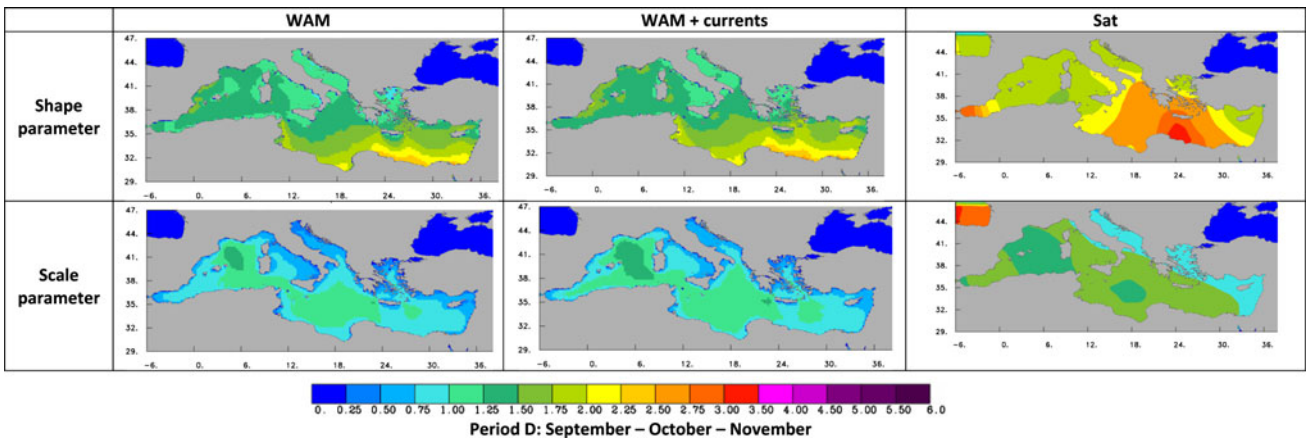

Fig. 13 The *shape* and *scale* parameter for the two model versions: with (WAMC) and without (WAM) current information, as well as for the corresponding satellite records for the months September–November

Estimating the deviations between WAM forecasts and satellite measurements

In this section a first attempt to apply the information geometric techniques described earlier for estimating the divergences between the wave model outputs and the corresponding satellite measurements is made. As already discussed in "Probability density function fitting", both data sets follow Weibull distributions. As a result, they can be categorized within the statistical manifold of all 2-parameter Weibull distributions:

$$S = \left\{ p(x;\xi) = \frac{\alpha}{\beta}\left(\frac{x}{\beta}\right)^{\alpha-1} e^{-\left(\frac{x}{\beta}\right)^{\alpha}};\quad \alpha \text{ and } \beta > 0 \right\} \tag{12}$$

The log-likelihood function here is:

$$\begin{aligned}\ell(x;\xi) &= \log[p(x;\xi)] \\ &= \log a - \log b + (a-1)(\log x - \log b) - \left(\frac{x}{\beta}\right)^{\alpha}\end{aligned} \tag{13}$$

and the Fisher information matrix, that defines the geometric entities of the manifold, takes the form:

$$G(\alpha,\beta) = \begin{bmatrix} \alpha^2\beta^2 & \beta(1-\gamma) \\ \beta(1-\gamma) & \frac{6(\gamma-1)^2+\pi^2}{6\alpha^2} \end{bmatrix} \tag{14}$$

where the constant $\gamma = \lim_{n\to+\infty}\left(\sum_{k=0}^{n}\frac{1}{n} - \ln n\right) \cong 0.577$ is the Euler Gamma. As a result, the Christoffel symbols of the Levi–Civita connection (see relations 7, 8) become:

$$\begin{aligned} \Gamma^1_{11} &= \frac{6\left(\gamma a - a - \frac{\pi^2}{6}\right)}{\pi^2\beta} & \Gamma^2_{11} &= \frac{-a^3}{\pi^2\beta^2} \\ \Gamma^1_{21} = \Gamma^1_{12} &= \frac{6\left(\gamma^2 - 2\gamma + \frac{\pi^2}{6} + 1\right)}{\pi^2 a} & \Gamma^2_{21} = \Gamma^2_{12} &= \frac{6a(1-\gamma)}{\pi^2\beta} \\ \Gamma^1_{22} &= -\frac{6(1-\gamma)\beta\left(\gamma^2 - 2\gamma + \frac{\pi^2}{6} + 1\right)}{\pi^2 a^3} & \Gamma^2_{22} &= -\frac{6\left(\gamma^2 - 2\gamma + \frac{\pi^2}{6} + 1\right)}{\pi^2 a} \end{aligned} \tag{15}$$

Within this framework, let's focus on the values obtained for October 2009 in the Levantine sea area. The shape and scale parameters for the WAM modeled values were $\alpha = 1.629$ and $\beta = 0.551$, respectively, for the WAMC version of the model $\alpha = 1.850$ and $\beta = 0.609$ and for the satellite corresponding records: $\alpha = 2.204$ and $\beta = 0.665$. Taking into account that these values do not deviate significantly, the probability density functions obtained can

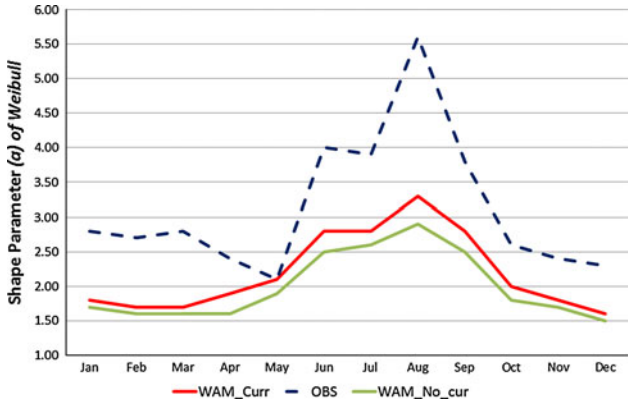

Fig. 14 The time evolution of the shape parameter in the Levantine area

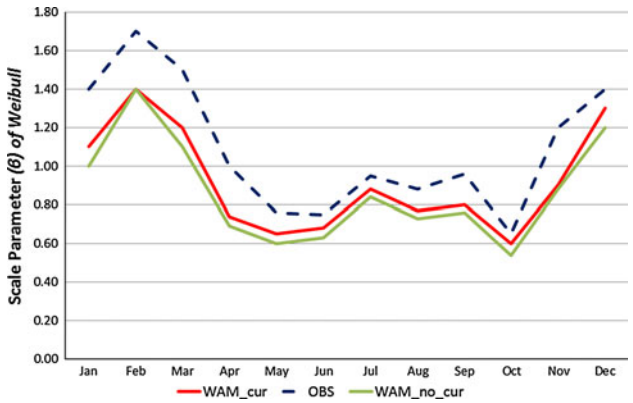

Fig. 15 The time evolution of the scale parameter in the Levantine area

Table 4 Monthly shape and scale parameter values and the corresponding 95% confidence intervals for the WAM (no currents) version at the area of Levantine

Weibull parameters	Jan	Feb	Mar	Apr	May	Jun	Jul	Aug	Sep	Oct	Nov	Dec
α (Shape parameter)	1.600	1.500	1.462	1.564	1.533	2.333	2.557	3.099	2.418	1.629	1.446	1.435
β (Scale parameter)	1.010	1.400	1.132	0.695	0.608	0.633	0.837	0.716	0.754	0.551	0.892	1.216
95% Confidence intervals for α	Jan	Feb	Mar	Apr	May	Jun	Jul	Aug	Sep	Oct	Nov	Dec
Min		1.594	1.491	1.457	1.558	1.528	2.324	2.547	3.087	2.409	1.620	1.441	1.430
Max		1.606	1.502	1.468	1.570	1.539	2.342	2.566	3.111	2.427	1.632	1.452	1.441
95% Confidence intervals for β	Jan	Feb	Mar	Apr	May	Jun	Jul	Aug	Sep	Oct	Nov	Dec
Min		1.011	1.391	1.128	0.693	0.606	0.631	0.835	0.715	0.753	0.549	0.885	1.211
Max		1.017	1.401	1.136	0.698	0.610	0.634	0.838	0.717	0.756	0.553	0.895	1.220

Table 5 Monthly shape and scale parameter values and the corresponding 95% confidence intervals for the WAM (currents) version at the area of Levantine

Weibull parameters	Jan	Feb	Mar	Apr	May	Jun	Jul	Aug	Sep	Oct	Nov	Dec
α (Shape parameter)	1.726	1.571	1.578	1.719	1.608	2.542	2.688	3.341	2.580	1.850	1.499	1.512
β (Scale parameter)	1.095	1.464	1.225	0.754	0.661	0.680	0.876	0.759	0.800	0.609	0.919	1.283
95% Confidence intervals for α	Jan	Feb	Mar	Apr	May	Jun	Jul	Aug	Sep	Oct	Nov	Dec
Min		1.720	1.565	1.573	1.713	1.602	2.532	2.678	3.329	2.571	1.843	1.494	1.507
Max		1.733	1.578	1.584	1.725	1.613	2.551	2.697	3.353	2.589	1.857	1.505	1.518
95% Confidence intervals for β	Jan	Feb	Mar	Apr	May	Jun	Jul	Aug	Sep	Oct	Nov	Dec
Min		1.092	1.459	1.221	0.752	0.658	0.679	0.874	0.758	0.798	0.607	0.916	1.279
Max		1.098	1.469	1.229	0.756	0.663	0.681	0.878	0.759	0.802	0.611	0.923	1.287

Table 6 Monthly shape and scale parameter values and the corresponding 95% confidence intervals for the satellite at the area of Levantine

Weibull parameters	Jan	Feb	Mar	Apr	May	Jun	Jul	Aug	Sep	Oct	Nov	Dec
α (Shape parameter)	2.523	2.450	2.560	2.140	1.576	3.759	3.515	4.938	3.491	2.204	1.911	2.208
β (Scale parameter)	1.441	1.762	1.509	1.012	0.780	0.759	0.960	0.889	0.968	0.665	1.224	1.442
95% Confidence intervals for α	Jan	Feb	Mar	Apr	May	Jun	Jul	Aug	Sep	Oct	Nov	Dec
Min		2.406	2.335	2.450	2.045	1.515	3.593	3.366	4.732	3.332	2.112	1.833	2.112
Max		2.646	2.570	2.676	2.239	1.639	3.933	3.671	5.152	3.657	2.301	1.992	2.310
95% Confidence intervals for β	Jan	Feb	Mar	Apr	May	Jun	Jul	Aug	Sep	Oct	Nov	Dec
Min		1.403	1.714	1.474	0.983	0.750	0.746	0.944	0.878	0.951	0.647	1.185	1.403
Max		1.480	1.810	1.545	1.042	0.811	0.772	0.977	0.900	0.986	0.684	1.265	1.482

be considered as elements $u_0 = W(1.629,\ 0.551)$, $u_1 = W(1.85,\ 0.609)$ and $u_2 = W(2.204,\ 0.665)$ of the statistical manifold S projected to the same tangent space $T_{u_1}S$ of u_1 where the corresponding inner product is given by the Fisher information matrix at u_1:

$$G = \begin{bmatrix} 1.85^2(0.609)^2 & 0.609(1-\gamma) \\ 0.609(1-\gamma) & \frac{6(\gamma-1)^2+\pi^2}{6\times 1.85^2} \end{bmatrix} = \begin{bmatrix} 1.27 & 0.26 \\ 0.26 & 0.53 \end{bmatrix}. \tag{16}$$

As a result, the distance between u_0 and u_2, that is the bias of the model, is given by:

$$d(u_0, u_2) = \sqrt{(u_0 - u_2)^T G (u_0 - u_2)} \tag{17}$$

which should replace the classical $\sqrt{(u_0 - u_2)^T (u_0 - u_2)}$ used by least square methods in conventional statistics.

Similarly, one can calculate the distance between any elements of the same tangent space. The novelty—comparing to the classical least square techniques—*is the use of the Fisher information matrix G instead of the identity*, which incorporates the geometrical structure of the manifold of distributions that fit to the data under study.

It is worth noticing, however, that the above approach can be applied only when the deviations between the pdfs in study are not major. When such an assumption cannot be made, the corresponding geodesics, i.e. the minimal length curves, should be employed. The latter are obtained as solutions of a system of 2nd order differential equations, under the conditions $\omega(0) = u_0, \omega(1) = u_2$. In the previous example, the utilization of the Christoffel symbols Γ^i_{jk} (Spivak 1965, 1979) obtained for the Weibull statistical manifold (Eq. 15), leads to the system:

$$\begin{aligned} &\omega_1''(t) + \frac{6\left(\gamma a - a - \frac{\pi^2}{6}\right)}{\pi^2\beta}\left(\omega_1'(t)\right)^2 + \frac{12\left(\gamma^2 - 2\gamma + \frac{\pi^2}{6} + 1\right)}{\pi^2 a} \\ &\omega_1'(t)\omega_2'(t) - \frac{6(1-\gamma)\beta\left(\gamma^2 - 2\gamma + \frac{\pi^2}{6} + 1\right)}{\pi^2 a^3}\left(\omega_2'(t)\right)^2 = 0, \\ &\omega_2''(t) - \frac{a^3}{\pi^2\beta^2}\left(\omega_1'(t)\right)^2 + \frac{12a(1-\gamma)}{\pi^2\beta}\omega_1'(t)\omega_2'(t) \\ &- \frac{6\left(\gamma^2 - 2\gamma + \frac{\pi^2}{6} + 1\right)}{\pi^2 a}\left(\omega_2'(t)\right)^2 = 0. \end{aligned} \tag{18}$$

It becomes obvious that such a system cannot be solved analytically, in general, and the use of some approximation method is necessary.

Conclusions

The wave characteristics in Mediterranean Sea by means of the swh values were studied based on different and independent sources: Two versions of the wave model WAM, one incorporating wind speed and sea currents as forcing and a second based only on wind speed, ran on a high spatial resolution mode (0.05°) for a period of one year (2009) providing detailed information over the whole Med sea. On the other hand, corresponding satellite measurements interpolated to gridded data were utilized based on the results of a recent European project (the Radar Altimetry project, Rosmorduc et al. 2009).

The obtained data were studied both by a conventional statistical point of view as well as by employing novel methodologies. The former approach includes a variety of statistical indices in order to have a clear view of the different data in study, to spot model biases as well as possible spatial and temporal variances. The latter employs tools obtained by a new branch of mathematics, the information geometry, in which the probability density functions are treated as elements of non-Euclidean structures avoiding simplifications made in classical statistics.

The main conclusions obtained can be summarized as follows:

- The use of surface currents does not result to major changes in the wave model outputs. Nevertheless, it does increase the mean values of the swh. The corresponding variability is also elevated at specific areas during winter months, indicating that one should not expect increased swh for the whole area or time of study. This point could be helpful for monitoring the wave power potential.
- The modeled data appear to have increased asymmetry, both in view of skewness and kurtosis, compared to the corresponding satellite values, especially during the summer period. This fact reveals increased influence of extreme values on the variability of the simulations. On the other hand questions on the smoothing and extrapolation procedures applied to the observations are raised.
- A more detailed study was performed for the swh in the homogeneous wave climate of the Levantine Sea. During the autumn period both the models and the observations coincide on increased values for the asymmetry measures. On the other hand, a slight but constant underestimation of the models is revealed which is improved when using sea currents information.
- In both cases (modeled and recorded data) a probability density function that fits well to the swh values is the two-parameter Weibull distribution. However, interesting deviations emerge for the shape and scale parameters:
  - Over the whole domain of study the satellite records emerge increased shape parameter values for the whole time period in study.
  - The spatial variability of the results is noticeable with main characteristic the increased shape and scale parameters in regions with relatively large potential fetch.
  - In the Levantine sea area particularly increased shape parameter values were emerged during the summer period.

The above points underline the different qualitative characteristics between the modeled and measured data as well as between different regions of the Mediterranean Sea. This fact should be taken into consideration in optimization procedures (assimilation, local adaptation, etc.). Towards this direction, some recent advances and statistical tools based on a new area of mathematics/statistics, the information geometry, have been discussed and tested in the last section of this work. New ways of estimating the distances between the data sets at hand are discussed avoiding the use of least square methods that de facto assume flat environments for the data in study. In particular, by employing the Weibull distributions that fit to the data sets at specific areas, a more detailed geometric environment is developed and concrete ways of distance estimation are proposed.

Acknowledgment This work was partially supported by the MARINA project (7th Framework Programme, Grant agreement number: 241402, http://www.marina-platform.info/), the E-wave project (funded by the Research Promotion Foundation of Cyprus, http://www.oceanography.ucy.ac.cy/ewave/) and the MyOcean project (European Marine Core Service, EU FP7, http://www.myocean.eu.org/).

References

Abdalla S, Bidlot J, Janssen P (2005a) Assimilation of ERS and ENVISAT wave data at ECMWF. ENVISAT & ERS symposium, Salzburg, 6–10 September 2004 (ESA SP-572, April 2005)

Abdalla S, Bidlot J, Janssen P (2005b) Jason altimeter wave height verification and assimilation. In: Proceedings of the seventh international conference on the Mediterranean coastal environment (MEDCOAST 05), Kusadasi, 25–29 October 2005, pp 1179–1185

Abdalla S, Janssen P, Bidlot J (2010) Jason-2 OGDR wind and wave products: monitoring, validation and assimilation. Mar Geodesy 33(1):239–255. doi:10.1080/01490419.2010.48779

Amari SI (1985) Differential geometrical methods in statistics. Springer lecture notes in statistics 28. Springer, Berlin

Amari SI, Nagaoka H (2000) Methods of information geometry. Oxford University Press, Oxford

Arwini K, Dodson CTJ (2007) Alpha-geometry of the weibull manifold. Second basic science conference, Tripoli

Arwini K, Dodson CTJ (2008) Information geometry: near randomness and near independence. Lecture notes in mathematics 1953. Springer, Berlin

Bertotti L, Bidlot J, Bunney C, Cavaleri L, Delli Passeri L, Gomez M, Lefevre JM, Paccagnella T, Torrisi L, Valentini A, Vocino A (2011) Performance of different forecast systems in an exceptional storm in the western Mediterranean Sea. Q J R Meteorol Soc. doi:10.1002/qj.892

Bidlot J, Janssen P, Abdalla S, Hersbach H (2007) A revised formulation of ocean wave dissipation and its model impact. ECMWF tech. memo. 509. ECMWF, Reading, p 27, available online at: http://www.ecmwf.int/publications/

Breivik LA, Reistad M (1994) Assimilation of ERS-1 altimeter wave heights in an operational numerical wave model. Weather Forecast 9:440–451

Chu PC, Cheng KF (2007) Effect of wave boundary layer on the sea-to-air dimethylsulfide transfer velocity during typhoon passage. J Marine Syst 66:122–129

Chu PC, Cheng KF (2008) South China Sea wave characteristics during Typhoon Muifa passage in winter 2004. J Oceanogr 64:1–21

Chu PC, Qi Y, Chen YC, Shi P, Mao QW (2004) South China Sea wave characteristics. Part-1: validation of wavewatch-III using TOPEX/poseidon data. J Atmos Ocean Technol 21(11):1718–1733

D'Agostino RB, Stephens MA (1986) Goodness-of-fit techniques. Marcel Dekker, New York

Dobricic S, Pinardi N (2008) An oceanographic three-dimensional variational data assimilation scheme. Ocean Model 22:89–105

Durrant TH, Greenslade D, Simmonds I (2009) Validation of Jason-1 and Envisat remotely sensed wave heights. J Atmos Ocean Sci 26:123–124

Emmanouil G, Galanis G, Kallos G, Breivik LA, Heilberg H, Reistad M (2007) Assimilation of radar altimeter data in numerical wave models: an impact study in two different wave climate regions. Ann Geophys 25(3):581–595

Enjolras V, Vincent P, Souyris JC, Rodriguez E, Phalippou L, Cazenave A (2006) Performances study of interferometric radar altimeters: from the instrument to the global mission definition. Sensors 6:164–192

Galanis G, Anadranistakis M (2002) A one dimensional Kalman filter for the correction of near surface temperature forecasts. Meteorol Appl 9:437–441

Galanis G, Louka P, Katsafados P, Kallos G, Pytharoulis I (2006) Applications of Kalman filters based on non-linear functions to numerical weather predictions. Ann Geophys 24:2451–2460

Galanis G, Emmanouil G, Kallos G, Chu PC (2009) A new methodology for the extension of the impact in sea wave assimilation systems. Ocean Dyn 59(3):523–535

Greenslade D, Young I (2005) The impact of inhomogenous background errors on a global wave data assimilation system. J Atmos Ocean Sci 10(2):61–93

Hasselmann K (1974) On the characterization of ocean waves due to white capping. Boundary-Layer Meteorol 6:107–127

Hasselmann S, Hasselmann K, Allender JH, Barnett TP (1985) Computations and parameterizations of the nonlinear energy transfer in a gravity wave spectrum. Part II: parameterizations of the nonlinear energy transfer for application in wave models. J Phys Oceanogr 15(11):1378–1391

Holthuijsen LH (2007) Waves in oceanic and coastal waters. Cambridge Univesity Press, Cambridge

Janssen P (2000) ECMWF wave modeling and satellite altimeter wave data. In: Halpern D (ed) Satellites, oceanography and society. Elsevier, NY, pp 35–36

Janssen P (2004) The interaction of ocean waves and wind. Cambridge University Press, Cambridge

Janssen P, Onorato M (2007) The intermediate water depth limit of the Zakharov equation and consequences for wave prediction. J Phys Oceanogr 37:2389–2400

Janssen P, Lionello P, Reistad M, Hollingsworth A (1987) A study of the feasibility of using sea and wind information from the ERS-1 satellite, part 2: use of scatterometer and altimeter data in wave modelling and assimilation. ECMWF report to ESA, Reading

Janssen P, Abdalla S, Hersbach H, Bidlot J (2007) Error estimation of buoy, satellite and model wave height data. J Atmos Ocean Technol 24:1665–1677

Kallos G (1997) The regional weather forecasting system SKIRON. In: Proceedings, symposium on regional weather prediction on parallel computer environments, 15–17 October 1997, Athens, p 9

Kalman RE (1960) A new approach to linear filtering and prediction problems. Trans ASME Ser D 82:35–45

Kalman RE, Bucy RS (1961) New results in linear filtering and prediction problems. Trans ASME Ser D 83:95–108

Kalnay E (2002) Atmospheric modeling, data assimilation and predictability. Cambridge University Press, New York

Komen G, Hasselmann S, Hasselmann K (1984) On the existence of a fully developed windsea spectrum. J Phys Oceanogr 14:1271–1285

Komen G, Cavaleri L, Donelan M, Hasselmann K, Hasselmann S, Janssen P (1994) Dynamics and modelling of ocean waves. Cambridge University Press, Cambridge

Lionello P, Günther H, Janssen P (1992) Assimilation of altimeter data in a global third generation wave model. J Geophys Res 97(C9):14453–14474

Lionello P, Günther H, Hansen B (1995) A sequential assimilation scheme applied to global wave analysis and prediction. J Marine Syst 6:87–107

Makarynskyy O (2004) Improving wave predictions with artificial neural networks. Ocean Eng 31(5–6):709–724

Makarynskyy O (2005) Neural pattern recognition and prediction for wind wave data assimilation. Pac Oceanogr 3(2):76–85

Muraleedharan G, Rao AD, Kurup PG, Unnikrishnan N, Mourani S (2007) Modified Weibull distribution for maximum and significant wave height simulation and prediction. Coast Eng 54:630–638

Papadopoulos A, Katsafados P, Kallos G (2001) Regional weather forecasting for marine application. Global Atmos Ocean Syst 8(2–3):219–237

Pinardi N, Allen I, De Mey P, Korres G, Lascaratos A, Le Traon PY, Maillard C, Manzella G, Tziavos C (2003) The Mediterranean ocean forecasting system: first phase of implementation (1998–2001). Ann Geophys 21(1):3–20

Rao ST, Zurbenko IG, Neagu R, Porter PS, Ku JY, Henry RF (1997) Space and time scales in ambient ozone data. Bull Am Meteor Soc 78(10):2153–2166

Rosmorduc V, Benveniste J, Lauret O, Maheu C, Milagro M, Picot N (2009) Radar altimetry tutorial. In: Benveniste J, Picot N (ed). http://www.altimetry.info

Spivak M (1965) Calculus on manifolds. W. A. Benjamin, New York

Spivak M (1979) A comprehensive introduction to differential geometry, vol 1–5, 2nd edn. Publish or Perish, Wilmington

Tonani M, Pinardi N, Adani N, Bonazzi A, Coppini G, De Dominicis M, Dobricic S, Drudi M, Fabbroni N, Fratianni C, Grandi A, Lyubartsev S, Oddo P, Pettenuzzo D, Pistoia J, Pujol I (2008) The Mediterranean ocean forecasting system, coastal to global operational oceanography: achievements and challenges. In: Proceedings of the fifth international conference on EuroGOOS 20–22 May 2008, Exeter

WAMDIG (The WAM-Development and Implementation Group), Hasselmann S, Hasselmann K, Bauer E, Bertotti L, Cardone CV, Ewing JA, Greenwood JA, Guillaume A, Janssen P, Komen G, Lionello P, Reistad M, Zambresky L (1988) The WAM model: a third generation ocean wave prediction model. J Phys Oceanogr 18(12):1775–1810

Yaplee BS et al (1971) Nanoseconds radar observations of the ocean surface from a stable platform. IEEE Trans Geosci Electron GE-9:171–174